Self-Organization of Action Hierarchy and Compositionality by Reinforcement Learning with Recurrent Networks

Dongqi Han
Cognitive Neurorobotics Research Unit
Okinawa Institute of Science and Technology
Okinawa, Japan
dongqi.han@oist.jp

Kenji Doya
Neural Computation Unit
Okinawa Institute of Science and Technology
Okinawa, Japan
doya@oist.jp

Jun Tani*
Cognitive Neurorobotics Research Unit
Okinawa Institute of Science and Technology
Okinawa, Japan
jun.tani@oist.jp

Abstract

Recurrent neural networks (RNNs) for reinforcement learning (RL) have shown distinct advantages, e.g., solving memory-dependent tasks and meta-learning. However, little effort has been spent on improving RNN architectures and on understanding the underlying neural mechanisms for performance gain. In this paper, we propose a novel, multiple-timescale, stochastic RNN for RL. Empirical results show that the network can autonomously learn to abstract sub-goals and can self-develop an action hierarchy using internal dynamics in a challenging continuous control task. Furthermore, we show that the self-developed compositionality of the network enhances faster re-learning when adapting to a new task that is a re-composition of previously learned sub-goals, than when starting from scratch. We also found that improved performance can be achieved when neural activities are subject to stochastic rather than deterministic dynamics.

1 Introduction

Reinforcement learning (RL) [Sutton and Barto, 1998] with neural networks as function approximators, i.e., deep RL, has undergone rapid development in recent years. State-of-the-art RL frameworks have shown proficient performance in various kinds of tasks, from game playing [Mnih et al., 2016, Silver et al., 2016, 2017] to continuous robot control [Lillicrap et al., 2015, Wang et al., 2017]. While most deep RL studies have employed feed-forward neural networks (FNNs) to solve tasks that can be well modeled by Markov Decision Processes (MDP) [Bellman, 1957], RL with recurrent neural networks (RNNs) has garnered increasing attention [Hausknecht and Stone, 2015, Heess et al., 2015, Shibata and Sakashita, 2015, Zhang et al., 2016, Al-Shedivat et al., 2018, Vezhnevets et al., 2017, Ha and Schmidhuber, 2018, Kapturowski et al., 2018, Wang et al., 2018].

One benefit of RNNs comes from their capacity to solve a kind of *Partially Observable MDPs* (POMDP) [Åström, 1965] in which optimal decision-making requires information derived from historical observations, i.e. memory-dependent tasks. While the curse of dimensionality [Friedman,

*Corresponding author

Preprint. Under review.

1997] occurs if these tasks are modelled into MDPs by including all historic information in the current state, a more tractable way of solving memory-dependent tasks is to leverage the contextual capacity of RNNs as function approximators [Schmidhuber, 1991]. [Wierstra et al., 2007, Utsunomiya and Shibata, 2008, Heess et al., 2015] have shown how RNNs enable successful RL in memory-dependent control tasks. Interestingly, even for tasks that are readily solved by MDPs, such as Atari games [Mnih et al., 2015], extraordinary performance can be achieved using relatively simple algorithms with RNNs [Kapturowski et al., 2018].

Furthermore, RNNs advance *meta-learning* in RL, defined as an effect that an agent requires statistically less time in learning to solve new tasks, compared to previously learned tasks, provided that the two tasks share some common elements [Thrun and Pratt, 1998, Wang et al., 2018, Frans et al., 2018]. Al-Shedivat et al. [2018] showed that meta-learning by robotic agents in dynamically changing tasks using recurrent policies, while Wang et al. [2018] argued that the prefrontal cortex, which contains many recurrent connections, plays an important role in meta-learning.

Despite successes of RL with RNN in relatively simple environments, solving more sophisticated tasks often requires cognitive competency in dealing with hierarchical operations, such as for composition/decomposition of an entire task from a sequence of sub-goals [Sutton et al., 1999, Dietterich, 2000, Bacon et al., 2017]. But very few studies have been devoted to developing hierarchical control utilizing RNN architectures. Vezhnevets et. al. [Vezhnevets et al., 2017] showed that multiple levels of RNN controllers with different temporal resolutions can achieve dramatic performance on difficult hierarchical RL tasks. However, their method requires one to assume a particular form of transition model for embedding sub-goals.

Inspired by [Yamashita and Tani, 2008], who showed emergence of a functional hierarchy in supervised learning using a multi-timescale RNN, we wondered how a multiple-timescale RNN can help to discover sequential sub-goal structure correlated with longer-term rewards using slower timescales, as well as to learn detailed actions characterized by faster timescales, via exploration-based RL?

In considering this problem, the current paper proposes a novel RL framework referred to as *Recurrent Multi-timescale Actor-critic with STochastic Experience Replay* (**ReMASTER**) as well a novel sequential compositional task for testing the performance of the framework. Two essential proposals in this framework are as follows:

The first is to employ a multiple timescale property in neural activation dynamics [Newell et al., 2001, Huys et al., 2004, Smith et al., 2006, Murray et al., 2014, Runyan et al., 2017], as well as in the discount factors across different levels in an RNN. Although it has been shown that introduction of multiple-timescale neural activation dynamics in RNNs enhances development of hierarchy in supervised learning [Yamashita and Tani, 2008], such a possibility in RL remains to be investigated. In most RL algorithms, the discount factor (for an MDP) [Sutton and Barto, 1998] is treated as a single hyper-parameter. However, [Tanaka et al., 2016, Enomoto et al., 2011] have shown that dopamine neurons in mammalian brains encode value functions with different region-specific discount factors. In considering motor control, it is intuitive that detailed motor skills are learned with a faster discounting (on the order of seconds), while abstracted actions for long-term plans require longer timescales. In summary, it is expected that more detailed information processing can autonomously develop at lower levels by incorporating the faster timescale constraints imposed on both neural activation dynamics and the reward discounting. Meanwhile, more abstracted action plans can develop at higher levels with slower timescale constraints.

The second proposal is to introduce stochasticity not only in motor outputs, but also in internal neural dynamics at all levels of RNN for generating exploratory behaviors. This is inspired by the fact that cortical neurons, which play a key role in intelligence, have highly stochastic firing behaviors, both for irregular inter-spike intervals and for noisy firing rates [Softky and Koch, 1993, Beck et al., 2008, 2012, Hartmann et al., 2015]. Chung et al. [2015], Fraccaro et al. [2016] have shown that various types of stochastic RNN models can learn to extract probabilistic structure hidden in temporal patterns by using variational Bayes approaches in supervised learning. It was also shown that stochastic FNNs facilitate efficient exploration and improved performance in RL [Fortunato et al., 2018, Florensa et al., 2017]. Therefore, we are interested in whether and how stochastic RNNs promote exploration and extraction of task features.

ReMASTER integrates these two essential ideas (multiple-timescale property and neuronal stochasticity) with an off-policy advantage actor-critic algorithm, in a model-free manner. We considered

a kind of sequential, compositional tasks in which an agent learns to accomplish a set of sub-goals in a specific sequence without being given prior knowledge about the sub-goals. The experimental results using ReMASTER showed that compositionality develops autonomously, accompanied by an emergence of hierarchical representation of actions in the network. More specifically, internal representations of task-relevant sub-goals were observed in the lower level, characterized by faster timescale dynamics, whereas sequential combination of those sub-goals into a global task goal was observed at the higher level characterized by the slower one.

We further examined performance of ReMASTER by considering a multi-phase relearning task wherein an agent is required to adapt consecutively to new tasks that constitute a re-composition of previous-occurred sub-goals. ReMASTER outperformed other alternatives by showing remarkable performance in relearning cases because it was able to utilize a previously learned representation about the sub-goals in a compositional way, thanks both to multiple timescales and neuronal stochasticity used in the model.

2 Methods

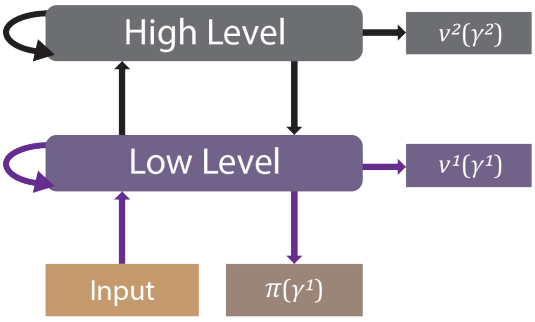

Figure 1: The basic structure of MTSRNN is shown for the case of a 2-level configuration, used in this work. However, additional levels can readily be stacked onto it.

We used a multi-level stochastic RNN with level-specific timescales, as a basic network architecture for implementing ReMASTER. This architecture is referred to as *Multiple Timescale Stochastic Recurrent Neural Network* (MTSRNN). Fig. 1 shows the case of a 2-level MTSRNN where and γ^l represents the characteristic discount factor at l-th level. v^l as the value function at l-th level is estimated by temporal difference learning (TD-learning) [Sutton and Barto, 1998] using the corresponding γ^l. While the policy function with discount factor γ^1, indicated by π, is estimated by the lowest level. Though the network has multiple timescales of discounting, γ^1 serves as the discount factor of the being optimized expected return. Also, only the lowest level receives inputs.

2.1 Multiple Timescale Stochastic RNN

Here we describe detailed mechanisms of L-levels MTSRNN. We use a super-script $l \in \{1, 2, \ldots, L\}$ to indicate the lth level, where a smaller l indicates a lower level. For level l, we have

$$\boldsymbol{u}^l(t) = (1 - \frac{1}{\tau^l})\boldsymbol{u}^l(t-1) + \frac{1}{\tau^l}\left[W_{cu}^{l-1,l}\boldsymbol{c}^{l-1}(t) + W_{cu}^{l,l}\boldsymbol{c}^l(t-1) + W_{cu}^{l+1,l}\boldsymbol{c}^{l+1}(t-1) + \boldsymbol{b}_u^l\right], \tag{1}$$

where $\boldsymbol{c}^{l-1}(t) = \boldsymbol{s}(t)$ when $l = 1$ is the current sensory input (state) and $\boldsymbol{c}^{l+1}$ does not exist for $l = L$. We informally call $\boldsymbol{u}$ as *hidden states* and $\boldsymbol{c}$ as *activated states*, and collectively call them *internal states*. The parameter τ^l is known as *timescale* of the lth level, which determines how fast hidden states vary, for which we used $\tau^1 = 2$ and $\tau^2 = 8$ throughout this study. Synaptic weights and biases, denoted by W and $\boldsymbol{b}$, respectively, are trainable parameters of the neural network. For all the levels, we have:

$$\boldsymbol{z}^l(t) = \boldsymbol{u}^l(t) + \boldsymbol{\epsilon}^l(t) \odot \boldsymbol{\sigma}^l(t), \tag{2}$$

$$\boldsymbol{c}^l(t) = \tanh\left(\boldsymbol{z}^l(t)\right), \tag{3}$$

where $\odot$ indicates element-wise production, and $\boldsymbol{\sigma}^l(t)$ is the scale of neuronal noise, which can be either a hyper-parameter or adaptive. And $\boldsymbol{\epsilon}^l(t)$ is a diagonal-covariance unit-Gaussian noise, which leads to a stochastic variable $\boldsymbol{z}^l(t)$ using the reparameterization trick [Kingma and Welling, 2013].

Value functions can be estimated via a linear connection from each level of the MTSRNN: $v^l(t) = (\boldsymbol{w}^l_{cv})^T \boldsymbol{c}^l(t) + b^l_{cv}$. We focus on continuous action space, so the policy function can be expressed as diagonal Gaussian distributions $\boldsymbol{\pi}(t) \sim \mathcal{N}\left(\boldsymbol{p}(t), \boldsymbol{e}(t)\right)$, where $\boldsymbol{p}(t) = \tanh\left(W_{ca}\boldsymbol{c}^1(t) + \boldsymbol{b}_{ca}\right)$ is the expected action assuming that the range of possible actions is $[-1, 1]$, and that $\boldsymbol{e}(t)$ is the exploration scale, which can be provided by experimenters or can be parameterized as: $\boldsymbol{e}(t) = \exp\left[\frac{1}{2}\left(W^l_{ce}\boldsymbol{c}^1(t) + \boldsymbol{b}^l_{ce}\right)\right]$. Although not illustrated in this work, this network can also output policy with respect to discrete actions, using softmax, as in [Mnih et al., 2016, Wang et al., 2017].

2.2 Off-Policy Advantage Actor-Critic

Recent deep RL studies using actor-critic algorithms with experience replay have achieved remarkable performance in many RL environments [Lillicrap et al., 2015, Wang et al., 2017, Haarnoja et al., 2018] by learning repetitively from previous experience. Therefore, for better sample efficiency, we use an off-policy actor-critic algorithm, which can deal with both continuous and discrete action spaces.

Suppose that in each episode, the agent is continuously interacting with the environment. At every step t, it experiences a state transition, which can be described by a tuple $(s_t, a_t, s_{t+1}, r_t, done_t, \pi(a_t|s_t))$, where s, a, r, π are state (observation), action, reward and policy function, respectively; and the Boolean $done_t$ indicates whether the episode ends at step $t+1$. The agent stores the state transition in a replay buffer. In practice, RNNs require initial states for computing succeeding time development of internal states. We set initial internal states to zero at the beginning of each episode. For easier access to initial states during experience replay using RNN, we also recorded $\boldsymbol{c}^l(t)$ and $\boldsymbol{u}^l(t)$ of the MTSRNN at each step are used them in experience replay[2].

For estimation of the critic, we used an off-policy version of the temporal difference (TD) learning algorithm [Sutton and Barto, 1998] to train value functions of all levels. Knowing that (i) each level has a characteristic timescale τ^l; (ii) $1/(1-\gamma)$ indicates the eigen-timescale of discounting [Doya, 2000], it is natural to set the values of discount factors as

$$\gamma^l = 1 - \frac{K}{\tau^l}, \tag{4}$$

where K is a constant to which we assigned a value of 0.16 throughout this work.

Let $\boldsymbol{\theta}$ denote the synaptic weights of the network. At each update, we randomly sample N state transition tuples from memory, and then conduct stochastic gradient descent for value functions v^l:

$$\boldsymbol{\theta} \leftarrow \boldsymbol{\theta} + \alpha_v \frac{1}{L}\frac{1}{N}\sum_l^L \sum_i^N \left[\rho_i \delta^l_i \nabla_{\boldsymbol{\theta}} v^l(\boldsymbol{s}_{0:\tau_i}; \boldsymbol{\theta})\right], \tag{5}$$

where α_v is learning rate for v, and $\rho_i = \frac{\pi(\boldsymbol{a}_{\tau_i}|\boldsymbol{s}_{0:\tau_i};\boldsymbol{\theta})}{\pi(\boldsymbol{a}_{\tau_i}|\boldsymbol{s}_{0:\tau_i};\boldsymbol{\theta}_{old})}$ and $\delta^l_i = r_{\tau_i} + \gamma^l v^l(\boldsymbol{s}_{0:\tau_i+1};\boldsymbol{\theta}) - v^l(\boldsymbol{s}_{0:\tau_i};\boldsymbol{\theta})$ are the importance sampling ratio and the TD-error for the ith sample and the lth level, respectively. Note that the value function v^l depends on $\boldsymbol{s}_{0:\tau_i}$ because we consider memory-dependent task.

To update the policy function, an advantage policy gradient algorithm was used in an off-policy manner [Degris et al., 2012], where the advantage was estimated by 1-step TD error with discount factor γ^1.

$$\boldsymbol{\theta} \leftarrow \boldsymbol{\theta} + \alpha_a \frac{1}{N}\sum_i^N \left[\rho_i \delta^1_i \nabla_{\boldsymbol{\theta}} \log \boldsymbol{\pi}(\boldsymbol{a}_{\tau_i}|\boldsymbol{s}_{0:\tau_i};\boldsymbol{\theta})\right], \tag{6}$$

[2]The recorded internal states can be incompatible with the current RNN as learning goes on. However, this issue does not impact learning performance much because very old samples are discarded due to limited memory. We took this approach because of its simplicity (More discussion in Appendix A3.2).

Algorithm 1 ReMASTER

Initialize the MTSRNN $\mathcal{R}$ and the replay buffer $\mathcal{B}$, global step $t \leftarrow 0$
repeat
  Reset an episode, assign $\mathcal{R}$ with zero internal states $(\boldsymbol{u}_t^l, \boldsymbol{z}_t^l) \leftarrow \mathbf{0}$.
  while episode not terminated **do**
    Obtain policy π_t by computing 1-step forward of $\mathcal{R}$ with current state s_t
    Sample an action a_t from π_t and execute a_t
    Record $(s_t, a_t, s_{t+1}, r_t, done_t)$, π_t and $(\boldsymbol{u}_t^l, \boldsymbol{z}_t^l)$ into $\mathcal{B}$
    if $mod(t, train\_interval) == 0$ **then**
      Sample a batch of sequential training samples to update $\mathcal{R}$ by Eq. 5 and 6
    end if
    $t \leftarrow t + 1$
  end while
until training stopped

where α_a is the learning rate for the actor. Algorithm 1 shows the overall procedure of ReMASTER. We followed algorithm 1 for all experiments in this work.

3 Results

We applied 2-levels ReMASTER to a so-called *sequential target-reaching task*. The following explains the details of task designs and simulation results and their analysis for a basic task, followed by those for an extended task that deals with relearning of consecutive task wherein goal changes.

3.1 Sequential Target-Reaching Task

We propose a sensory-motor task, inspired by [Utsunomiya and Shibata, 2008], referred to as a "sequential target-reaching task". As illustrated in Fig. 2(a), a two-wheeled robot agent on a 2-dimensional field is required to reach three target positions, in a sequence, red-green-blue, without receiving any signal indicating which target to reach. The action is given by the rotation of its left and right wheels. At the beginning of each episode, the robot and targets are randomly placed on the field. The robot has sensors detecting distances and angles from the three targets, as well as the current-step reward. When it reaches a target in the correct sequence, it receives a one-step reward. The reward is given only if the agent followed the proper sequence, and is given only once for each target. An episode terminates if the agent completes the task or a maximum of 128 steps are taken. To successfully solve the task, the agent needs to develop the cognitive capability to remember "which target has been reached", as well as to recognize the correct sub-goal (which can be considered as approaching a target in this task).

The sequential target-reaching task is of particular interest because it abstracts many real-world tasks in complicated environments, which involve decomposition of a whole task into sub-tasks and execution of each sub-task in a specific sequence. One example is dialing on a classic telephone, where one needs to sequentially choose each number and perform detailed hand movements to dial the number. Mastering this kind of task naturally requires development of hierarchical control of actions. Lower levels acquire skills for action primitives, while higher levels learn to dispatch those action primitives in a specified sequence.

We examined ReMASTER in the sequential target-reaching task. For exploration. We applied Gaussian noise to both hidden states and motor actions, and annealed them exponentially with respect to episodes. Fig. 2(b) shows that ReMASTER can successfully solve this task through motor babbling, achieving more than 95% success rate[3] on average after training.

However, our major aim was to examine what sorts of internal representation the MTSRNN had developed for achieving sequential hierarchical control after abundant training using ReMASTER. Fig. 2(c) shows three examples of how an agent behaved after learning, where the three columns present the behavior of the same agent, but in different episodes. Interestingly, although target configurations were completely different in these episodes, high-level neurons showed relatively

[3] An episode was considered successful when the agent completed the task within 40 steps.

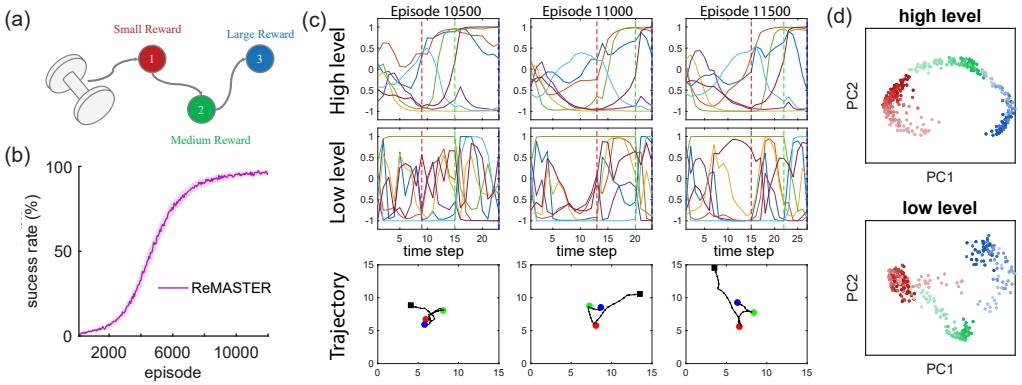

Figure 2: Sequential target-reaching task. (**a**) Illustration of the task. (**b**) Performance curve indicated by success rate. Shaded areas indicate 99% confidence interval, obtained from 50 repeats for ReMASTER and 10 repeats for PPO-LSTM. (**c**) Three example episodes showing the behavior of a well-trained ReMASTER agent. The first and second rows show activated hidden states $\boldsymbol{c}_t^l$ of two levels, where dashed lines indicate the agent's having reached a target. For clarity, we plotted only c_t^l of the first 7 neurons for both levels, with different colors indicating different neurons. The third row is the robot's trajectories, where black squares indicate its starting positions and circles are target positions. (**d**) PCA for visualizing temporal profiles of $\boldsymbol{c}_t^l$, using data of the same agent in (c) after convergence. Colors mean the agent is approaching to the corresponding targets, where a deeper color means the agent is more closed to the target. See Appendix A2.2 for more examples.

similar temporal profiles of activated hidden states $\boldsymbol{c}_t^l$, as plotted in the first row of Fig. 2(c). In contrast, this feature was less obvious in the lower level (second row of Fig. 2(c)). Although we could only show one agent here, this result is statistically significant (See Appendix A2.6). This result suggests that an MTSRNN with slower dynamics in the higher level enhanced development of a consistent representation, accounting for a given sub-goal structure through abstraction in the higher level, whereas the lower level dealt with details of motor control depending on object configuration in the field in each episode. Consistency in representing sub-goals of the higher level can also be demonstrated by conducting PCA on activated hidden states of the two levels of the MTSRNN after convergence (Fig. 2(d)). We can see that the high-level activated hidden states showed a consistent, sequence-like representation of sub-goals accounted by its slower dynamics, whereas the lower level showed a more divergent representation [Yang et al., 2019] since it needs to generate each different maneuvering trajectory. Hence, we saw an emergence of action hierarchy using ReMASTER.

3.2 Consecutive Relearning Task

Since our previous analysis indicated that the low level learns action primitives for achieving each sub-goal, relearning to solve a new task that is a re-composition of previously learned sub-goals in a different sequence, should be much easier than starting from scratch.

By considering this, we carried out another experiment, in an extended version of the sequential target-reaching task, referred to as an "consecutive relearning task" (Fig. 3(a)). In this task, the robot agent was required to adapt consecutively to changed task goals (or more specifically, changed reward functions and termination conditions) by relearning. The consecutive relearning task consisted of 3 different phases. Phase 1 corresponded to the original red-green-blue sequential target-reaching task. Phases 2 and 3 appeared as novel re-compositions of sub-goals, where the required sequences are green-blue-red and blue-green-red, respectively. There were 12,000 episodes in phase 1, and 4,000 in both phase 2 and phase 3.

We performed experiments on this task in a lifelong learning manner [Thrun and Mitchell, 1994, Silver et al., 2013]. We maintained the same learning algorithm and hyper-parameters throughout all 3 phases. Synaptic weights were continuously updated without resetting throughout the experiment. At the beginning of each phase, motor and neuronal noise were reset and the replay buffer was cleared. We compared performance using ReMASTER to two alternatives, in order to examine the importance

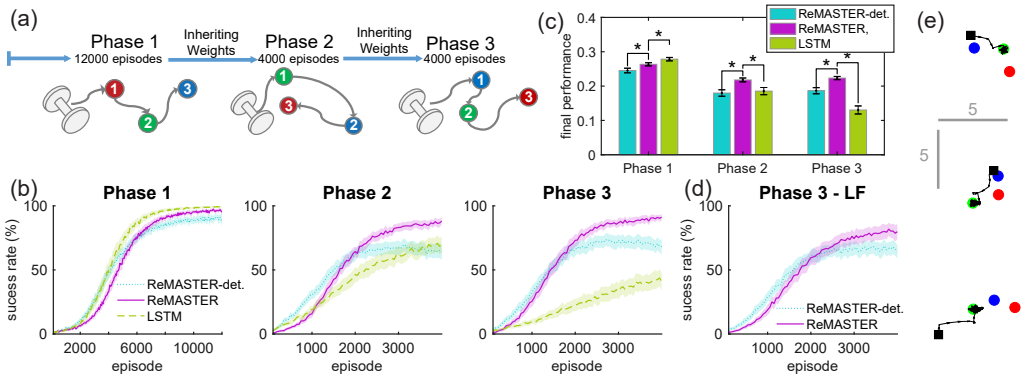

Figure 3: Consecutive relearning task and followed-up simulations. (**a**) Illustration of the task. (**b**) Performance curves for all phases, plotted in the same way as Fig. 2(b). (**c**) Comparison among different architectures, where the final performance is computed by averaging rewards over the last 1,000 episodes from 50 repeats. Error-bars show 99% confidence intervals, and a star indicates $p < 0.01$ for a two-sample t-test. (**d**) Performance curves for phase 3 with low-level synaptic weights frozen. (**e**) Manipulating the agent's behaviors by clamping high-level internal states in 3 random episodes, where the agent consistently executing the action primitive to approach the green target. Black squares indicate the agent's initial positions and colored circles indicate the targets.

of neuronal stochasticity and intrinsic timescale hierarchy. One alternative model is the deterministic version of ReMASTER in which there was no noise added to hidden states (ReMASTER-det. in Fig. 3(b, c, d)). Another alternative used the same algorithm, but replaced the MTSRNN with a single-layer LSTM (LSTM in Fig. 3(b, c)) using $\gamma = 1 - \sqrt{(1-\gamma^1)(1-\gamma^2)}$, but we got similar performance for $\gamma = \gamma^1$ or γ^2).

Results are illustrated in Fig. 3(b, c). Fig. 3(b) shows task performance in terms of success rate in three different phases. Fig. 3(c) shows final performance statistics indicated by mean rewards (total rewards divided by number of steps in each episode) in the same comparison. Several conclusions can be drawn from these results.

First, for ReMASTER and ReMASTER-det., the relearning cases of phases 2,3 starting with previously trained synaptic weights achieved much better sample efficiency than the case of phase 1 which was done from scratch (Note that there were only 4,000 episodes in phases 2,3, whereas there were 12,000 episodes in phase 1. Rigorous comparison is left to Appendix A2.4 due to page limits). We consider that this resulted from compositionality during action hierarchy development, which enabled a flexible re-composition of sub-goals, so that the agents could rapidly adapt to relearning tasks.

Second, ReMASTER significantly and consistently outperformed ReMASTER-det. in all the three phases (Fig. 3(b,c)). One possible reason is that stochastic neurons could prevent the network from over-fitting, thereby enhancing network flexibility. Another is that neuronal noise can lead to larger exploration in the hidden state space [Shibata and Sakashita, 2015, Fortunato et al., 2018], which results in a greater likelihood of finding adequate neural representation in the higher level, which fits with newly appeared re-composition tasks.

Finally, ReMASTER, as well as its deterministic version showed a performance advantage over the LSTM alternative in phase, although LSTM achieved great performance in phase 1 (Fig. 3(b)). We consider the performance degradation of LSTM in phase 3 is because of the mixed representation of sub-goal sequencing and detailed motor skills in one level. This created difficulty in relearning sub-goal sequencing while reusing low-level skills (Indeed, the performance degradation of LSTM is not specified in our implementation, but is also observed with other algorithms and implementations using LSTM (See Appendix A5)). In contrast, ReMASTER provided flexible compositionality that enables these two levels of control to be better segregated in different levels in MTSRNN. Although biological plausibility of our approach is arguable, this result may underlie a potential reason of why we have many separated, timescale-distinct brain regions [Murray et al., 2014, Runyan et al., 2017].

3.3 Learning to Solve New Tasks with Low-Level Weights Frozen

The previous results (Fig. 3(b)) were obtained when both higher and the lower level synaptic connections were continually developing throughout the task. However, if the low level had acquired necessary motor skills for achieving the sub-goals, it should be possible for the agent to learn to solve new tasks by updating only the higher level.

Therefore, we conducted another simulation on the consecutive relearning task using ReMASTER, in which low-level synaptic weights (purple connections in Fig. 1) were frozen in phase 3, as inherited at the end of phase 2. ReMASTER and ReMASTER-det. agents still achieved remarkable learning efficiency in phase 3 (Fig. 3(d)). This finding further supports our speculation that hierarchical action control had developed in phases 1 and 2, wherein motor skills for achieving sub-goals had developed in the low-level and memory for sequencing sub-goals had developed in the high-level.

3.4 Manipulating Agent Behaviors by Clamping High-Level Neural States

For animals, different brain regions often serve at different levels in action generation. For instance, premotor areas of rodent motor cortex are thought to be important in action choices, while primary motor cortex is considered responsible for details in action execution [Morandell and Huber, 2017]. More interestingly, experimental studies have demonstrated that action primitives of animals can be altered by electrophysiological stimulation or optogenetic inactivation to certain upstream neurons [Morandell and Huber, 2017, Vu et al., 1994].

Here, we consider analogous experiments on artifacts with ReMASTER agents. By fixing high-level internal states $(\boldsymbol{c}^2, \boldsymbol{u}^2)$ to particular values, we could "manipulate" a trained agent to consistently follow an action primitive pursuing the corresponding sub-goal (Fig. 3(e) shows the case of approaching the green target). In contrast, fixing low-level internal states only results in a constant (noisy) action, which is directly determined by $\boldsymbol{c}^1$. Therefore, the high-level internal states act as a label for the action primitives. The continuous property of the internal states enables representation of an arbitrary number of sub-goals, where in our case we can readily find 3 meaningful action primitives corresponding to the 3 targets (See Appendix A2.5 for details).

4 Related Work

Despite much early effort spent on hierarchical RL [Sutton et al., 1999, Dietterich, 2000] using pre-defined action hierarchies, a number of recent studies have been focused on discovering action primitives[4] that serves for hierarchical RL. [Brunskill and Li, 2014, Bacon et al., 2017, Fox et al., 2017, Riemer et al., 2018] were extensions of the *option* framework [Sutton et al., 1999], which requires a pre-defined number of options, whereas our framework can learn to represent an arbitrary number of options by high-level internal states (Fig. 3(e)). Moreover, most of these studies were based on MDPs or semi-MDPs [Sutton et al., 1999], where it does not require long-term credit assignment or memorization. In this paper, we consider a different scheme wherein the agent needs to accomplish a series of sub-goals in a particular sequence without observable information indicating the current sub-goal. Such a scheme is common in real life, but has rarely been investigated in RL.

Another track of related studies is skill sharing/reuse among similar tasks in RL. Studies have been conducted considering various schemes, such as meta-RL [Santoro et al., 2016, Finn et al., 2017, Al-Shedivat et al., 2018, Finn et al., 2018, Kim et al., 2018, Wang et al., 2018] and lifelong RL [Silver et al., 2013, Mankowitz et al., 2016, Rusu et al., 2016, Tessler et al., 2017, Abel et al., 2018]. In particular, some authors proposed ideas shared with our work. Santoro et al. [2016], Al-Shedivat et al. [2018], Wang et al. [2018] employed RNNs for their meta-learning competency, and Brunskill and Li [2014], Tessler et al. [2017] suggested that reuse of action primitives can enhance lifelong learning. However, many of these works considered a multi-task setting where the agent repetitively interacts with a random task sampled from a task set. In our case, the agent first learned to solve one task (phase 1), and the self-developed action hierarchy facilitated relearning in new tasks (phases 2 and 3) with which the agents had never interacted.

[4] "Action primitive" in our paper has a similar meaning as *option* [Sutton et al., 1999] in some related literature [Bacon et al., 2017, Brunskill and Li, 2014, Bacon et al., 2017, Fox et al., 2017]

5 Conclusion and Future Work

In the current study, we focused on a type of sequential compositional task and comprehensively investigated how they can be solved by autonomously developing sub-goal structure with acquiring necessary action primitives via RL. For this purpose, we proposed a novel RL framework, ReMASTER, which is characterized by two essential features. One is the multiple timescale property both in neural activation dynamics and reward discounting, which is inspired by neuroscientific findings [Newell et al., 2001, Huys et al., 2004, Smith et al., 2006, Murray et al., 2014, Runyan et al., 2017]. The other is stochastic noise introduced in neural units in all layers, as inspired by [Beck et al., 2008, 2012, Orbán et al., 2016].

Simulation results showed that action hierarchy emerged by developing an adequate internal neuronal representation at multiple levels. We presented several pieces of evidences showing that compositionality developed in the network by taking advantage of multiple timescales: abstract action control in terms of sequencing of sub-goals developed in the higher level, while a set of action primitives as skills for detailed sensory-motor control for achieving each sub-goal acquired in the lower level.

Furthermore, compositionality developed in the previous learning enabled efficient relearning in adaptation to changed task goals that involved re-composition of previously learned sub-goals. This re-composition capability was further enhanced with introduction of neuronal noise in addition to motor noise. Such adaptation became possible because development of hierarchical control using multiple levels allowed enough flexibility for re-composition of previously learned control skills.

Indeed, our preliminary experiment showed that exchange of timescales between the higher and lower levels resulted in significant performance degradation. It should be worth investigating how an optimal timescale for each level can be determined autonomously during task execution. One possibility is to incorporate LSTMs cascaded in multiple levels [Vezhnevets et al., 2017] with the expectation that the forgetting gate in LSTMs could provide the means for adaptive timescale modulation.

Also, ReMASTER is flexible in adopting any gradient-based actor-critic algorithms. Performance can be improved by employing well-designed algorithms such as [Wang et al., 2017, Haarnoja et al., 2018], as well as by adding a target network for a soft-update of value functions [Mnih et al., 2015].

Finally, recent model-based RL methods have addressed promising performance using probabilistic state transition models [Deisenroth and Rasmussen, 2011, Ha and Schmidhuber, 2018]. Among such methods, a prominent one is probabilistic inference with a Bayesian RNN [Gal et al., 2016]. In this respect, it should be interesting to combine ReMASTER with probabilistic inference of state transitions [Schmidhuber, 2018], using, e.g., a multiple timescale Bayesian RNN [Ahmadi and Tani, 2018]. Such trials will be attempted in future studies.

Acknowledgements

This work was supported by OIST Graduate School funding. We would like to thank Katsunari Shibata, Tadashi Kozuno and Siqing Hou for insightful discussions.

References

Richard S Sutton and Andrew G Barto. *Reinforcement learning: An introduction*, volume 1. MIT press Cambridge, 1998.

Volodymyr Mnih, Adria Puigdomenech Badia, Mehdi Mirza, Alex Graves, Timothy Lillicrap, Tim Harley, David Silver, and Koray Kavukcuoglu. Asynchronous methods for deep reinforcement learning. In *International Conference on Machine Learning*, pages 1928–1937, 2016.

David Silver, Aja Huang, Chris J Maddison, Arthur Guez, Laurent Sifre, George Van Den Driessche, Julian Schrittwieser, Ioannis Antonoglou, Veda Panneershelvam, Marc Lanctot, et al. Mastering the game of go with deep neural networks and tree search. *nature*, 529(7587):484, 2016.

David Silver, Julian Schrittwieser, Karen Simonyan, Ioannis Antonoglou, Aja Huang, Arthur Guez, Thomas Hubert, Lucas Baker, Matthew Lai, Adrian Bolton, et al. Mastering the game of go without human knowledge. *Nature*, 550(7676):354, 2017.

Timothy P Lillicrap, Jonathan J Hunt, Alexander Pritzel, Nicolas Heess, Tom Erez, Yuval Tassa, David Silver, and Daan Wierstra. Continuous control with deep reinforcement learning. *arXiv preprint arXiv:1509.02971*, 2015.

Ziyu Wang, Victor Bapst, Nicolas Heess, Volodymyr Mnih, Remi Munos, Koray Kavukcuoglu, and Nando de Freitas. Sample efficient actor-critic with experience replay. 2017.

Richard Bellman. A Markovian decision process. *Journal of Mathematics and Mechanics*, pages 679–684, 1957.

Matthew Hausknecht and Peter Stone. Deep recurrent Q-learning for partially observable mdps. *CoRR, abs/1507.06527*, 7(1), 2015.

Nicolas Heess, Jonathan J Hunt, Timothy P Lillicrap, and David Silver. Memory-based control with recurrent neural networks. *arXiv preprint arXiv:1512.04455*, 2015.

Katsunari Shibata and Yuta Sakashita. Reinforcement learning with internal-dynamics-based exploration using a chaotic neural network. In *Neural Networks (IJCNN), 2015 International Joint Conference on*, pages 1–8. IEEE, 2015.

Marvin Zhang, Zoe McCarthy, Chelsea Finn, Sergey Levine, and Pieter Abbeel. Learning deep neural network policies with continuous memory states. In *2016 IEEE International Conference on Robotics and Automation (ICRA)*, pages 520–527. IEEE, 2016.

Maruan Al-Shedivat, Trapit Bansal, Yuri Burda, Ilya Sutskever, Igor Mordatch, and Pieter Abbeel. Continuous adaptation via meta-learning in nonstationary and competitive environments. 2018.

Alexander Sasha Vezhnevets, Simon Osindero, Tom Schaul, Nicolas Heess, Max Jaderberg, David Silver, and Koray Kavukcuoglu. Feudal networks for hierarchical reinforcement learning. In *Proceedings of the 34th International Conference on Machine Learning-Volume 70*, pages 3540–3549. JMLR. org, 2017.

David Ha and Jürgen Schmidhuber. Recurrent world models facilitate policy evolution. In S. Bengio, H. Wallach, H. Larochelle, K. Grauman, N. Cesa-Bianchi, and R. Garnett, editors, *Advances in Neural Information Processing Systems 31*, pages 2450–2462. Curran Associates, Inc., 2018. URL `http://papers.nips.cc/paper/7512-recurrent-world-models-facilitate-policy-evolution.pdf`.

Steven Kapturowski, Georg Ostrovski, Will Dabney, John Quan, and Remi Munos. Recurrent experience replay in distributed reinforcement learning. *OpenReview*, 2018.

Jane X Wang, Zeb Kurth-Nelson, Dharshan Kumaran, Dhruva Tirumala, Hubert Soyer, Joel Z Leibo, Demis Hassabis, and Matthew Botvinick. Prefrontal cortex as a meta-reinforcement learning system. *Nature neuroscience*, 21(6):860, 2018.

Karl J Åström. Optimal control of Markov processes with incomplete state information. *Journal of Mathematical Analysis and Applications*, 10(1):174–205, 1965.

Jerome H Friedman. On bias, variance, 0/1—loss, and the curse-of-dimensionality. *Data mining and knowledge discovery*, 1(1):55–77, 1997.

Jürgen Schmidhuber. Reinforcement learning in Markovian and non-Markovian environments. In *Advances in neural information processing systems*, pages 500–506, 1991.

Daan Wierstra, Alexander Foerster, Jan Peters, and Juergen Schmidhuber. Solving deep memory pomdps with recurrent policy gradients. In *International Conference on Artificial Neural Networks*, pages 697–706. Springer, 2007.

Hiroki Utsunomiya and Katsunari Shibata. Contextual behaviors and internal representations acquired by reinforcement learning with a recurrent neural network in a continuous state and action space task. In *International Conference on Neural Information Processing*, pages 970–978. Springer, 2008.

Volodymyr Mnih, Koray Kavukcuoglu, David Silver, Andrei A Rusu, Joel Veness, Marc G Bellemare, Alex Graves, Martin Riedmiller, Andreas K Fidjeland, Georg Ostrovski, et al. Human-level control through deep reinforcement learning. *Nature*, 518(7540):529, 2015.

Sebastian Thrun and Lorien Pratt. Learning to learn: Introduction and overview. In *Learning to learn*, pages 3–17. Springer, 1998.

Kevin Frans, Jonathan Ho, Xi Chen, Pieter Abbeel, and John Schulman. Meta learning shared hierarchies. 2018.

Richard S Sutton, Doina Precup, and Satinder Singh. Between mdps and semi-mdps: A framework for temporal abstraction in reinforcement learning. *Artificial intelligence*, 112(1-2):181–211, 1999.

Thomas G Dietterich. Hierarchical reinforcement learning with the maxQ value function decomposition. *Journal of Artificial Intelligence Research*, 13:227–303, 2000.

Pierre-Luc Bacon, Jean Harb, and Doina Precup. The option-critic architecture. In *Thirty-First AAAI Conference on Artificial Intelligence*, 2017.

Yuichi Yamashita and Jun Tani. Emergence of functional hierarchy in a multiple timescale neural network model: a humanoid robot experiment. *PLoS computational biology*, 4(11):e1000220, 2008.

Karl M Newell, Yeou-Teh Liu, and Gottfried Mayer-Kress. Time scales in motor learning and development. *Psychological review*, 108(1):57, 2001.

Raoul Huys, Andreas Daffertshofer, and Peter J Beek. Multiple time scales and multiform dynamics in learning to juggle. *Motor control*, 8(2):188–212, 2004.

Maurice A Smith, Ali Ghazizadeh, and Reza Shadmehr. Interacting adaptive processes with different timescales underlie short-term motor learning. *PLoS biology*, 4(6):e179, 2006.

John D Murray, Alberto Bernacchia, David J Freedman, Ranulfo Romo, Jonathan D Wallis, Xinying Cai, Camillo Padoa-Schioppa, Tatiana Pasternak, Hyojung Seo, Daeyeol Lee, et al. A hierarchy of intrinsic timescales across primate cortex. *Nature neuroscience*, 17(12):1661, 2014.

Caroline A Runyan, Eugenio Piasini, Stefano Panzeri, and Christopher D Harvey. Distinct timescales of population coding across cortex. *Nature*, 548(7665):92, 2017.

Saori C Tanaka, Kenji Doya, Go Okada, Kazutaka Ueda, Yasumasa Okamoto, and Shigeto Yamawaki. Prediction of immediate and future rewards differentially recruits cortico-basal ganglia loops. In *Behavioral economics of preferences, choices, and happiness*, pages 593–616. Springer, 2016.

Kazuki Enomoto, Naoyuki Matsumoto, Sadamu Nakai, Takemasa Satoh, Tatsuo K Sato, Yasumasa Ueda, Hitoshi Inokawa, Masahiko Haruno, and Minoru Kimura. Dopamine neurons learn to encode the long-term value of multiple future rewards. *Proceedings of the National Academy of Sciences*, page 201014457, 2011.

William R Softky and Christof Koch. The highly irregular firing of cortical cells is inconsistent with temporal integration of random epsps. *Journal of Neuroscience*, 13(1):334–350, 1993.

Jeffrey M Beck, Wei Ji Ma, Roozbeh Kiani, Tim Hanks, Anne K Churchland, Jamie Roitman, Michael N Shadlen, Peter E Latham, and Alexandre Pouget. Probabilistic population codes for Bayesian decision making. *Neuron*, 60(6):1142–1152, 2008.

Jeffrey M Beck, Wei Ji Ma, Xaq Pitkow, Peter E Latham, and Alexandre Pouget. Not noisy, just wrong: the role of suboptimal inference in behavioral variability. *Neuron*, 74(1):30–39, 2012.

Christoph Hartmann, Andreea Lazar, Bernhard Nessler, and Jochen Triesch. Where's the noise? key features of spontaneous activity and neural variability arise through learning in a deterministic network. *PLoS computational biology*, 11(12):e1004640, 2015.

Junyoung Chung, Kyle Kastner, Laurent Dinh, Kratarth Goel, Aaron C Courville, and Yoshua Bengio. A recurrent latent variable model for sequential data. In *Advances in neural information processing systems*, pages 2980–2988, 2015.

Marco Fraccaro, Søren Kaae Sønderby, Ulrich Paquet, and Ole Winther. Sequential neural models with stochastic layers. In *Advances in neural information processing systems*, pages 2199–2207, 2016.

Meire Fortunato, Mohammad Gheshlaghi Azar, Bilal Piot, Jacob Menick, Ian Osband, Alex Graves, Vlad Mnih, Remi Munos, Demis Hassabis, Olivier Pietquin, et al. Noisy networks for exploration. 2018.

Carlos Florensa, Yan Duan, and Pieter Abbeel. Stochastic neural networks for hierarchical reinforcement learning. In *Proceedings of the International Conference on Learning Representations (ICLR)*, 2017.

Diederik P Kingma and Max Welling. Auto-encoding variational Bayes. *arXiv preprint arXiv:1312.6114*, 2013.

Tuomas Haarnoja, Aurick Zhou, Pieter Abbeel, and Sergey Levine. Soft actor-critic: Off-policy maximum entropy deep reinforcement learning with a stochastic actor. In *International Conference on Machine Learning*, pages 1856–1865, 2018.

Kenji Doya. Reinforcement learning in continuous time and space. *Neural computation*, 12(1): 219–245, 2000.

Thomas Degris, Martha White, and Richard Sutton. Off-policy actor-critic. In *International Conference on Machine Learning*, 2012.

Guangyu Robert Yang, Madhura R Joglekar, H Francis Song, William T Newsome, and Xiao-Jing Wang. Task representations in neural networks trained to perform many cognitive tasks. *Nature neuroscience*, 22(2):297, 2019.

Sebastian Thrun and Tom M Mitchell. Learning one more thing. Technical report, Carnegie-Mellon Univ Pittsburgh PA Dept of computer science, 1994.

Daniel L Silver, Qiang Yang, and Lianghao Li. Lifelong machine learning systems: Beyond learning algorithms. In *AAAI Spring Symposium: Lifelong Machine Learning*, volume 13, page 05, 2013.

Karin Morandell and Daniel Huber. The role of forelimb motor cortex areas in goal directed action in mice. *Scientific reports*, 7(1):15759, 2017.

Eric T Vu, Mark E Mazurek, and Yu-Chien Kuo. Identification of a forebrain motor programming network for the learned song of zebra finches. *Journal of Neuroscience*, 14(11):6924–6934, 1994.

Emma Brunskill and Lihong Li. PAC-inspired option discovery in lifelong reinforcement learning. In *International Conference on Machine Learning*, pages 316–324, 2014.

Roy Fox, Sanjay Krishnan, Ion Stoica, and Ken Goldberg. Multi-level discovery of deep options. *arXiv preprint arXiv:1703.08294*, 2017.

Matthew Riemer, Miao Liu, and Gerald Tesauro. Learning abstract options. In *Advances in Neural Information Processing Systems*, pages 10424–10434, 2018.

Adam Santoro, Sergey Bartunov, Matthew Botvinick, Daan Wierstra, and Timothy Lillicrap. Meta-learning with memory-augmented neural networks. In *International conference on machine learning*, pages 1842–1850, 2016.

Chelsea Finn, Pieter Abbeel, and Sergey Levine. Model-agnostic meta-learning for fast adaptation of deep networks. In *International Conference on Machine Learning*, pages 1126–1135, 2017.

Chelsea Finn, Kelvin Xu, and Sergey Levine. Probabilistic model-agnostic meta-learning. In *Advances in Neural Information Processing Systems*, pages 9516–9527, 2018.

Taesup Kim, Jaesik Yoon, Ousmane Dia, Sungwoong Kim, Yoshua Bengio, and Sungjin Ahn. Bayesian model-agnostic meta-learning. *arXiv preprint arXiv:1806.03836*, 2018.

Daniel J Mankowitz, Timothy A Mann, and Shie Mannor. Adaptive skills adaptive partitions (asap). In *Advances in Neural Information Processing Systems*, pages 1588–1596, 2016.

Andrei A Rusu, Neil C Rabinowitz, Guillaume Desjardins, Hubert Soyer, James Kirkpatrick, Koray Kavukcuoglu, Razvan Pascanu, and Raia Hadsell. Progressive neural networks. *arXiv preprint arXiv:1606.04671*, 2016.

Chen Tessler, Shahar Givony, Tom Zahavy, Daniel J Mankowitz, and Shie Mannor. A deep hierarchical approach to lifelong learning in minecraft. In *Thirty-First AAAI Conference on Artificial Intelligence*, 2017.

David Abel, Yuu Jinnai, Sophie Yue Guo, George Konidaris, and Michael Littman. Policy and value transfer in lifelong reinforcement learning. In *International Conference on Machine Learning*, pages 20–29, 2018.

Gergő Orbán, Pietro Berkes, József Fiser, and Máté Lengyel. Neural variability and sampling-based probabilistic representations in the visual cortex. *Neuron*, 92(2):530–543, 2016.

Marc Deisenroth and Carl E Rasmussen. Pilco: A model-based and data-efficient approach to policy search. In *Proceedings of the 28th International Conference on machine learning (ICML-11)*, pages 465–472, 2011.

Yarin Gal, Rowan McAllister, and Carl Edward Rasmussen. Improving pilco with Bayesian neural network dynamics models. In *Data-Efficient Machine Learning workshop, ICML*, volume 4, 2016.

Jürgen Schmidhuber. One big net for everything. *arXiv preprint arXiv:1802.08864*, 2018.

Ahmadreza Ahmadi and Jun Tani. Learning to embed probabilistic structures between deterministic chaos and random process in a variational Bayes predictive-coding rnn. *arXiv preprint arXiv:1811.01339*, 2018.

Richard S Sutton, David A McAllester, Satinder P Singh, and Yishay Mansour. Policy gradient methods for reinforcement learning with function approximation. In *Advances in neural information processing systems*, pages 1057–1063, 2000.

Matteo Hessel, Joseph Modayil, Hado Van Hasselt, Tom Schaul, Georg Ostrovski, Will Dabney, Dan Horgan, Bilal Piot, Mohammad Azar, and David Silver. Rainbow: Combining improvements in deep reinforcement learning. In *Thirty-Second AAAI Conference on Artificial Intelligence*, 2018.

Andrew G Barto, Richard S Sutton, and Charles W Anderson. Neuronlike adaptive elements that can solve difficult learning control problems. *IEEE transactions on systems, man, and cybernetics*, pages 834–846, 1983.

Geoffrey Hinton, Nitish Srivastava, and Kevin Swersky. Rmsprop: Divide the gradient by a running average of its recent magnitude. *Neural networks for machine learning, Coursera lecture 6e*, 2012.

George E Uhlenbeck and Leonard S Ornstein. On the theory of the brownian motion. *Physical review*, 36(5):823, 1930.

John Schulman, Filip Wolski, Prafulla Dhariwal, Alec Radford, and Oleg Klimov. Proximal policy optimization algorithms. *arXiv preprint arXiv:1707.06347*, 2017.

Sepp Hochreiter and Jurgen Schmidhuber. Long short-term memory. *Neural computation*, 9(8): 1735–1780, 1997.

Prafulla Dhariwal, Christopher Hesse, Oleg Klimov, Alex Nichol, Matthias Plappert, Alec Radford, John Schulman, Szymon Sidor, Yuhuai Wu, and Peter Zhokhov. OpenAI Baselines. `https://github.com/openai/baselines`, 2017.

Ashley Hill, Antonin Raffin, Maximilian Ernestus, Adam Gleave, Rene Traore, Prafulla Dhariwal, Christopher Hesse, Oleg Klimov, Alex Nichol, Matthias Plappert, Alec Radford, John Schulman, Szymon Sidor, and Yuhuai Wu. Stable baselines. `https://github.com/hill-a/stable-baselines`, 2018.

Appendix A1 Neuronal Stochasticity

Existing popular RL frameworks [Sutton et al., 2000, Mnih et al., 2015, 2016, Wang et al., 2017, Hessel et al., 2018] mostly exploit motor babbling in terms of stochasticity in the action output, to explore the environment. We have demonstrated the basic framework of ReMASTER, where exploration is conducted with a probabilistic policy function. However, it is also possible to perform RL with internal-dynamic-based exploration in neural network approximators [Shibata and Sakashita, 2015].

Previous studies have suggested that more efficient exploration can be achieved by exploring the abstracted action scenario [Sutton et al., 1999]. It has been shown that in a multi-level RNN model, internal states are closely related to abstracted action patterns [Yamashita and Tani, 2008]. With the hypothesis that the RNN can encode an abstracted action scenario, we applied Gaussian white noise to hidden states to enhance exploration of novel action patterns so as to improve learning in hierarchical tasks.

Indeed, learning with stochastic neurons is contained in a regular advantage policy gradient algorithm[5] [Sutton et al., 2000, Degris et al., 2012], which considers maximizing the objective function by gradient ascent on parameters $\boldsymbol{\theta}$,

$$\nabla_\theta J(\boldsymbol{\theta}) = \mathbb{E}_{\boldsymbol{a}\sim\pi}\left[\hat{A}_\pi \nabla_\theta \log \pi(\boldsymbol{a})\right], \tag{7}$$

where $\hat{A}_\pi$ is an estimation of the advantage function $Q_\pi - V_\pi$. In ReMASTER, it is the TD-error of level 1: $\hat{A}_\pi = \delta_t^1 = r_t + \gamma V_{t+1}^1 - V_t^1$.

However, when RNN neurons are stochastic, we have the policy function

$$\pi = \pi(\boldsymbol{a}|\boldsymbol{c}, \boldsymbol{\theta}), \tag{8}$$

where $\boldsymbol{c}$ indicates the hidden states of the RNN, and $\boldsymbol{\theta}$ are the synaptic weights.

In stochastic RNN, the distribution of $\boldsymbol{c}$ given state $\boldsymbol{s}$ and $\boldsymbol{\theta}$ is:

$$\eta = \eta(\boldsymbol{c}|\boldsymbol{s}, \boldsymbol{\theta}). \tag{9}$$

Then Eq. 7 need to be re-written as:

$$\nabla_\theta J(\boldsymbol{\theta}) = \mathbb{E}_{\boldsymbol{c}\sim\eta,\boldsymbol{a}\sim\pi}\left[\hat{A}_\pi \nabla_\theta \log\left(\pi(\boldsymbol{a}|\boldsymbol{c})\eta(\boldsymbol{c})\right)\right] \tag{10}$$

$$= \mathbb{E}_{\boldsymbol{c}\sim\eta,\boldsymbol{a}\sim\pi}\left[\hat{A}_\pi (\nabla_\theta \log \pi(\boldsymbol{a}|\boldsymbol{c}) + \nabla_\theta \log \eta(\boldsymbol{c}))\right] \tag{11}$$

The first term $\hat{A}_\pi \nabla_\theta \log \pi(\boldsymbol{a}|\boldsymbol{c})$ is the policy gradient, given $\boldsymbol{c}$. Note that the first term does not have recurrent connections; thus, training of recurrent weights is reflected in the second term, $\hat{A}_\pi \nabla_\theta \log \eta(\boldsymbol{c})$, which has a similar form to a policy gradient. Thus we assume that by adding neuronal noise, learning performance can be improved by exploring internal states space, just as in a policy gradient, for either on-policy or off-policy learning.

Appendix A2 Experiments

A2.1 Sequential Target-Reaching Task

The setting for a sequential target-reaching task is similar to that in [Utsunomiya and Shibata, 2008]. A two-wheel robot is required to approach three targets in a sequence, on a 2-dimensional field, as showed in Fig. A4. The 2-D field is a 15×15 square area, restrained by walls. The robot agent has two wheels of radius 0.25, connected by an axle. It receives sensory signals to detect distances and angles to the target as well as the walls, as shown in Fig. A4. At each step, the action is given as the rotations of two wheels, which are continuous in range $[-180°, 180°]$. Length of the axle is 1, so that the robot can turn $90°$ at most in one step. There are three targets, indicated by red, green and blue, each of which is a circular area of radius 0.4. At the beginning of each episode, positions of three

[5] For clarity, here we consider the on-policy case, but it is straightforward to extend it to the off-policy case.

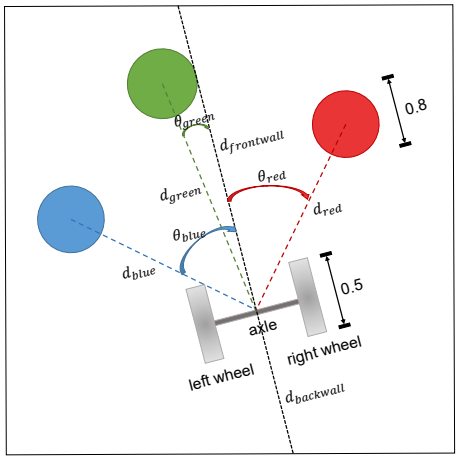

Figure A4: Top view of the sequential target-reaching task. Objects are zoomed out for visual clarity.

targets are randomly set inside the center 8×8 area. The distance between two targets are ensured to be larger than 2. The observation is a 12-D real number vector: $(e^{-d_{red}/5}, e^{-d_{green}/5}, e^{-d_{blue}/5}, e^{-d_{frontwall}/5}, e^{-d_{backwall}/5}, r, \sin\theta_{red}, \cos\theta_{red}, \sin\theta_{green}, \cos\theta_{green}, \sin\theta_{blue}, \cos\theta_{blue})$, where r is the immediate reward at current time step, and other quantities are shown in Fig. A4.

The robot must reach the three targets in the sequence red-green-blue to maximize rewards. The reward function is given as:

If $d_{red}(\tau) > 0.4\,\forall\,\tau < t$ and $d_{red}(t) \leq 0.4$, then

$$r(t) = 0.8/(1 + d_{red}(t)). \tag{12}$$

If $\exists\,\tau < t$ that $d_{red}(\tau) \leq 0.4$, and $d_{green}(\tau) > 0.4\,\forall\,\tau < t$, $d_{green}(t) \leq 0.4$, then

$$r(t) = 2.0/(1 + d_{green}(t)). \tag{13}$$

If $\exists\,\tau < t$ that $d_{red}(\tau) \leq 0.4$, and $\exists\,\tau < t$ that $d_{green}(\tau) \leq 0.4$, and $d_{blue}(t) \leq 0.4$, then

$$r(t) = 5.0/(1 + d_{green}(t)) \quad \text{(task done)}. \tag{14}$$

If the robot hits the walls, a negative reward -0.1 is given. Otherwise the reward is zero.

For exploration, we applied auto-correlated Gaussian noises to the robot's actions, which were generated by independent OU-processes. Each action noise x_t can be computed by

$$x_t = -\theta_a x_{t-1} + e\sqrt{2\theta_a}\epsilon_t, \tag{15}$$

where $\theta_a = 0.3$ for all of our experiments, and ϵ_t is a unit of Gaussian white noise. e indicates the scale of action noise, which was annealed exponentially with episodes, with a minimum value of 0.1:

$$e = 180^\circ \times [\exp(-0.0003 \times \text{episode}) + 0.1]\,. \tag{16}$$

Meanwhile, neuronal stochasticity is given by Gaussian white noise with scale

$$\sigma = \sigma_0 \exp(-0.0003 \times \text{episode}). \tag{17}$$

We performed experiments to determine the proper value of σ_0, and found that $\sigma_0 = 0.2$ gave rise to better performance (Fig. A10(a)). Thus we used $\sigma_0 = 0.2$ for ReMASTER.

The only difference between ReMASTER and **ReMASTER-det.** is that σ_0 in **ReMASTER-det.** is given as zero.

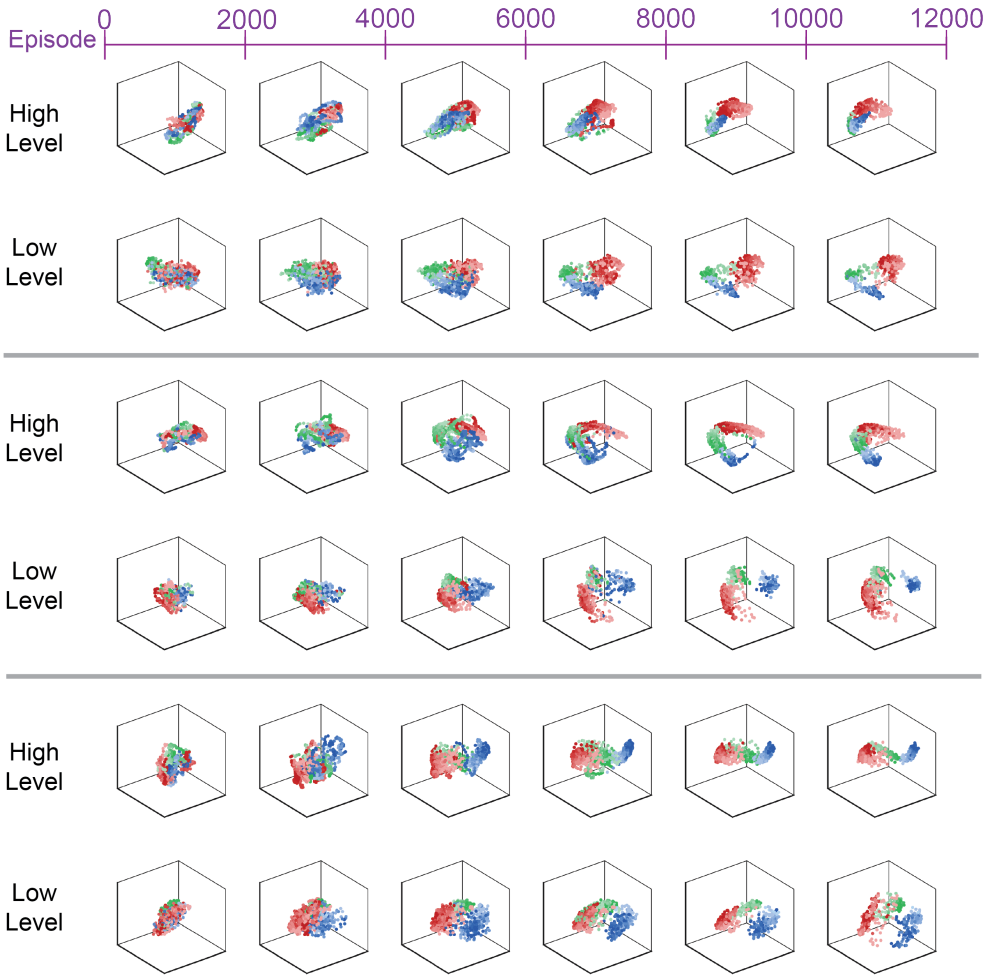

Figure A5: PCA visualizations of development of activated hidden states of ReMASTER agents in the sequential goal reaching task. The three axes indicates the first 3 PCs.

A2.2 PCA for activated hidden states

Data for the PCA plot in Fig. 2(d) were selected from episodes 10000, 10100, ..., 11900, where internal dynamics of MTSRNN had almost converged. Here we plotted three more examples (each from one agent with a different random seed) in Fig. A5, so that readers may have a more intuitive understanding of the internal dynamics developed during the sequential goal reaching task.

A2.3 Consecutive Relearning Task

In the consecutive relearning task, sensory observations for the robot are given consistently across all 3 phases. However, the only difference is that the reward function in each phase appears different. In phase 2, the robot needs to reach three targets according to the sequence green-blue-red, and in phase 3 the required sequence is blue-green-red.

Phase 1 had 12000 episodes, while phases 2 and 3 had 4000. At the beginning of phases 2 and 3, we cleared the memory buffer and reset the noise, annealed as

$$e = 180^\circ \times [\exp(-0.0009 \times \text{episode}) + 0.1]\,, \tag{18}$$

and

$$\sigma = \sigma_0 \exp(-0.0009 \times \text{episode}). \tag{19}$$

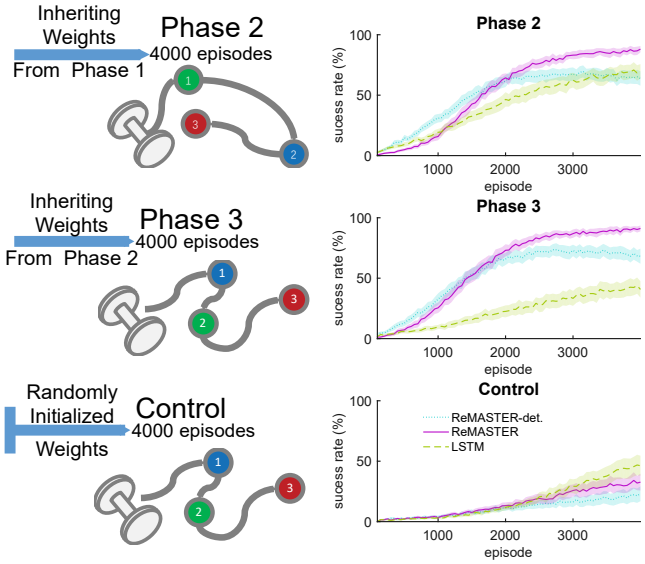

Figure A6: Performance comparison among phases 2, 3 and the control case, plotted in the same way as Fig. 3(b).

A2.4 Performance Gain with Inherited weights

we prepared a control task that is equal to phase 3 (also equivalent to phase 2 because of symmetry of the three targets) except a random initialization of synaptic weights at the beginning (Fig. A6 bottom). It can be seen that agents with inherited weights largely outperformed agents in the control case that start from scratch, showing meta-learning competency of RNNs [Wang et al., 2018].

A2.5 Manipulating Agent Behaviors by Clamping High-Level Internal States

We show more examples of manipulating agent behaviors by clamping high-level internal states in Fig. A7. We first randomly picked an agent after finishing the consecutive relearning task and then computed the average of $\boldsymbol{c}^2$ and $\boldsymbol{u}^2$ over the last 500 episodes of phase 3, at the middle step of (i) from initial position to the blue target (ii) from the blue target to the green one (iii) from the green target to the red one, and clamped $\boldsymbol{c}^2$ and $\boldsymbol{u}^2$ to these values in random new episodes. (i), (ii) and (iii) correspond to three rows of Fig. A7, respectively. And the examples shown in Fig. 3(e) were using (ii).

A2.6 Consistency in representing sub-goals

To understand the underlying neural mechanisms for ReMASTER's promising performance in relearning phases (Fig. 3(b,c)), we analyzed neural data by looking at how consistent the internal states of different RNN architectures could represent sub-goals.

Because there are usually different numbers of time steps in each episode, we first normalized the number of time steps to 30 for all successful episodes. The normalized time step $t_n = 1$ when the agent starts an episode, and $t_n = 10, 20$ and 30 when the agent reaches the first, second, and third target, respectively. Then $\boldsymbol{c}^l_{t_n}$ can be obtained with respect to the normalized time steps by linear interpolation. Therefore, if the higher-level activated hidden states can consistently represent the correct sub-goals, their temporal profiles $\boldsymbol{c}^2_{t_n}$ using normalized time steps should be similar among different episodes e after convergence.

We measured consistency in representing sub-goals by cosine similarity of $\boldsymbol{c}^l_{t_n}$:

$$\text{Consistency}^l = \text{Mean}_{e_i \neq e_j, t_n, k} \left[\text{CosSim} \left(c^l_{e_i,k,t_n}, c^l_{e_j,k,t_n} \right) \right], \tag{20}$$

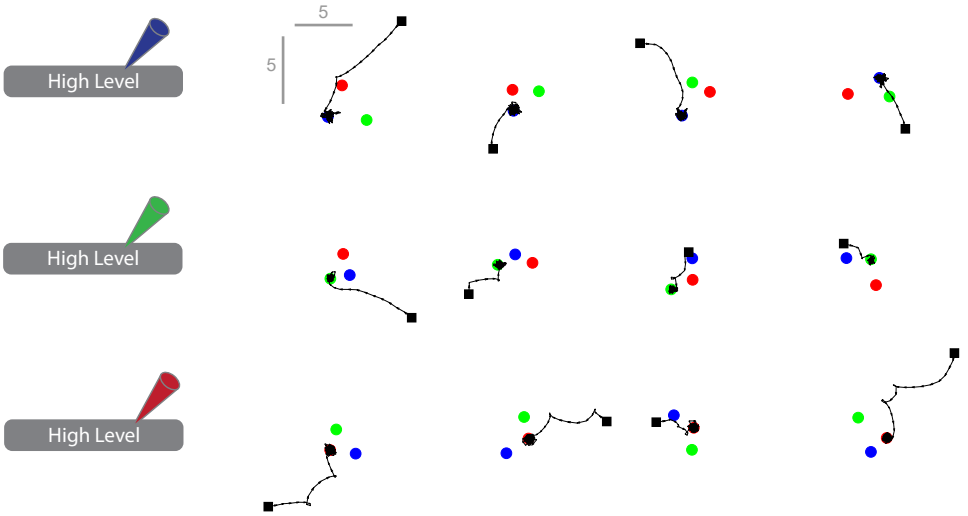

Figure A7: Manipulating agent behaviors by clamping high-level internal states. All trajectories were from one agent and each row used same high-level internal states. Black squares and colored circles indicate the agent's initial positions and the target positions, respectively.

Table A1: Consistency of activated hidden states in representing sub-goals among the last 2,000 episodes in each phase. Data are Mean±STD.

Network	ReMASTER-det.		ReMASTER		LSTM
	Low level	High level	Low level	High level	
Phase 1	0.75 ± 0.05	$\mathbf{0.88 \pm 0.04}$	0.73 ± 0.05	$\mathbf{0.91 \pm 0.03}$	$\mathbf{0.82 \pm 0.14}$
Phase 2	0.68 ± 0.06	0.82 ± 0.06	0.74 ± 0.05	$\mathbf{0.89 \pm 0.04}$	0.64 ± 0.20
Phase 3	0.70 ± 0.06	0.82 ± 0.06	0.76 ± 0.04	$\mathbf{0.91 \pm 0.03}$	0.50 ± 0.32

where $\boldsymbol{c}^{l}_{e,k,t_n}$ indicates the temporal profile (using the normalized time step t_n) of the internal state of the kth neuron of the lth level in the eth episode. e_i and e_j are successful episodes in the last 2,000 episodes of each phase.

Accordingly, we computed consistency in representing sub-goals of both of the higher level and the lower one (Table A1). It can been seen that higher consistency basically corresponds to higher success rate for the three models in the consecutive relearning task (Fig. 3(b,c)), where ReMASTER agents maintained high consistency in representing sub-goals in the higher level, in contrast to LSTM agents, the performance and consistency of which decreased significantly in later phases.

A2.7 Partially Observable Classic Control

We also performed experiments on partially observable (PO) classic control tasks [Heess et al., 2015], where velocities cannot be observed. The agent must infer velocities from its position and joint angles from observation of continuous time steps. An RNN makes it possible to use only the current step observation as input for the function approximator.

As the most typical control task for RL, *Cartpole* [Barto et al., 1983] was used to test our framework. In Cartpole, it is required to keep a cart carrying a pole on a 1-dimensional slideway from falling down by pushing it either left or right. The observable information in PO-cartpole is only the position of the cart and the angle of the pole. We performed experiments using the continuous-action version of PO-cartpole, where the action space is continuous from -1 to 1. Also, because the agent cannot infer initial velocities (for pole angle and cart position), they are given as zero. The result is shown in A8(a). ReMASTER learned more slowly than the **LSTM** alternative, but both succeeded in balancing it for more than 300 steps on average, given only current joint angle and position.

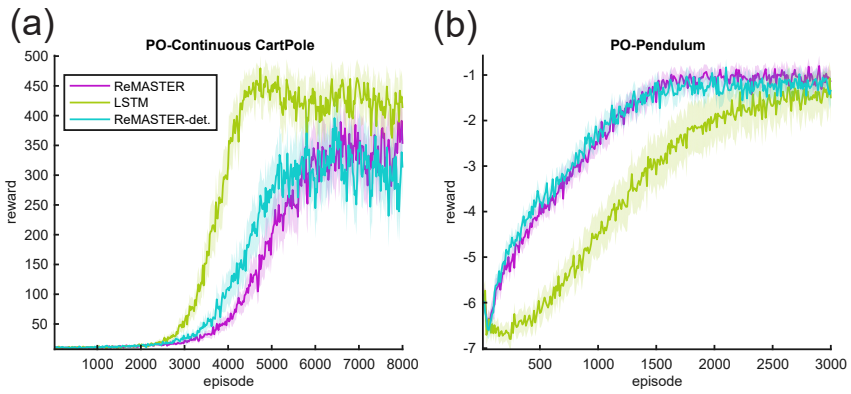

Figure A8: Results on (**a**) PO-continuous CartPole; (**b**) PO-Pendulum, where 95 % confidence interval is plotted as the shaded area, which was obtained from 50 repeats. For PO-CartPole, the reward is considered as the number of time steps the agent can balance until a maximum step of 500. For pendulum, the reward is given by step-wise mean rewards in an episode, where each episode has 200 steps.

Pendulum is another classic fine-control task often used to test RL algorithms, which requires the controller to swing the pendulum up and keep it on the top by applying a torque at each time step. In the usual setting of a pendulum environment, both its angle and angular velocity can be observed, but PO-pendulum conceals angular velocity from the agent. The network input we used for pendulum was the sine and cosine functions of current joint angle. Fig. A8(b) shows the result of ReMASTER and its rivals for PO-pendulum. Both the MTSRNN and LSTM can finally learn the near-optimal policy, while MTSRNN learns faster, probably due to its simpler dynamics.

We provided motor and neuronal noise in the same way as in the sequential target-reaching task. For ReMASTER in PO-cartpole,

$$e = \exp(-0.0004 \times \text{episode}) + 0.1, \tag{21}$$

and

$$\sigma = 0.2 \times \exp(-0.0004 \times \text{episode}). \tag{22}$$

For ReMASTER in PO-pendulum,

$$e = 2 \times [\exp(-0.001 \times \text{episode}) + 0.1], \tag{23}$$

and

$$\sigma = 0.2 \times \exp(-0.001 \times \text{episode}). \tag{24}$$

Appendix A3 Experience Replay with RNNs

A3.1 Replay Buffer for Dispersed Replay

To enable experience replay, we stored state transitions $(s_t, s_{t+1}, a_t, r_t, done_t)$ and internal states $(\boldsymbol{c}_t, \boldsymbol{\mu}_t)$ in a replay buffer. We also recorded behavior policy π_t in it to compute the importance sampling ratio. We did not separate episodes in the replay buffer. Instead, we consecutively recorded every step, and padded $L-1$ steps at which gradient descent needed to be stopped, when an episode terminated. Then, we could randomly sample n sequences of length-l as a minibatch for truncated BPTT, with all sampled steps having equal probability to be sampled to all BPTT steps.

A3.2 Initial internal states for Experience Replay

Different from feedforward neural networks, RNNs for off-policy RL have some practical problems. One major problem is how to decide initial states when training a sequence sampled from the replay buffer. When dealing with finite horizon (episodic) RL tasks, applicable approaches can be summarized as:

- **Recording the internal states at each step.** Internal states can be treated as hidden observations used in training, which need to be recorded in the replay buffer. Despite the simplicity of this approach, it is unclear what algorithmic issues will be introduced by difference between old internal representations and new ones.
- **Using an entire episode as a sequence.** This was used, e.g., in [Mnih et al., 2016], providing zero initial states for all the episodes. However, this implementation is computationally inefficient when the length of some episodes is large.
- **Using random sequences with zero initial states.** Sample sequences are randomly sampled from the entire memory, given all-zero initial states. This approach was used in [Hausknecht and Stone, 2015] for experiments in Atari Games. Unfortunately, this implementation prevents learning long-term dependence because of the mismatch of initial states, as argued in [Kapturowski et al., 2018].
- **Replaying the sequences.** Starting with zero initial states at each episode, internal states for off-policy updates can be obtained by unrolling new RNNs on old trajectories. A modified version of this approach is offered in [Kapturowski et al., 2018], where the authors assume that computing the forward dynamic of RNNs can help them find better internal states from zero or recorded internal states, starting e.g., 20 steps before the start of a sampled sequence. Although [Kapturowski et al., 2018] demonstrated remarkable performance on many RL tasks using this approach, their assumption has not been systematically discussed.

For simplicity, we employ the first approach. Our experimental results show that it is practical. However, how to choose better initial states still remains a challenge for RL with experience replay using RNNs.

Appendix A4 Implementation Details

These experiments were run on CentOS Linux machines using 12-core 2.50 GHz Intel Xeon E5-2680v3 processors. Codes were written with Python 3.6 using TensorFlow library. We used an MTSRNN with 2 levels for ReMASTER in all experiments, where $\tau^1 = 2$ and $\tau^2 = 8$. The discount factors are $\gamma^1 = 0.92, \gamma^2 = 0.98$, computed from $\gamma^l = 1 - 0.16/\tau^l$. There are 100 neurons in the lower level and 50 in the higher level. We directly used the observations as input to the low level RNN. We applied truncated BPTT of length 25 for the sequential target-reaching task, as well as the consecutive relearning task, and length 10 for partially observable CartPole and Pendulum.

We compared ReMASTER to two alternatives. One is **ReMASTER-det.**, to which neuronal noise was not applied. The other uses the same algorithm, but reduces two levels to a single level, and replaces the MTSRNN with a single-layer RNN that contained 75 regular LSTM cells (the **LSTM** alternative). The **LSTM** alternative was conducted with $\gamma^{LSTM} = 0.96$, computed from $\gamma^{LSTM} = 1 - 0.16/\sqrt{\tau^1\tau^2}$.

Otherwise, we used the same hyper-parameters for all experiments. Two separate RMSProp optimizers [Hinton et al., 2012] with decay 0.99 were used to minimize the losses of actor and critic, where learning rates were 0.0003 for $\mathcal{L}_\mathcal{V}$ and 0.0001 for $\mathcal{L}_\mathcal{A}$. We used a replay buffer of maximum size 500,000 and performed experience replay every 2 steps, using a mini-batch containing 16 dispersed sequences randomly sampled from the buffer.

Most of the hyper-parameters were obtained by a combination of hand-tuning and random search, and we summarized the hyper-parameters used in this study in Table A2. However, a different choice of hyper-parameters does not significantly change our main conclusions in Section 3.2 (Fig. A12).

A4.1 Temporally correlated motor noise

For continuous sensory-motor tasks, the range of state space can be very large. To enhance efficiency of motor exploration, we used motor noise generated by the *Ornstern-Uhlenbeck process* [Uhlenbeck and Ornstein, 1930] (OU-process), like that used in [Lillicrap et al., 2015]. The OU-process generates temporally auto-correlated noise; thus, the exploration range can be increased with the "inertia" of the noise. However, it is not necessary to apply temporally correlated noise to hidden states of the MTSRNN, since recurrent connections in an RNN autonomously generate it. In our all of our simulations, the inverse timescale of the OU-process θ_{OU} = 0.3 was used.

Table A2: Hyper-parameters we used in the sequential goal reaching task and the consecutive relearning task for ReMASTER.

Hyper-parameter	Description	Value
γ^1	Low-level discount factor	0.92
γ^2	High-level discount factor	0.98
τ^1	Low-level RNN timescale	2
τ^2	High-level RNN timescale	8
N^1	Number of neurons in the lower level	100
N^2	Number of neurons in the higher level	50
buffer_Size	Number of steps recorded in the memory	500,000
σ_0	Initial scale of neuronal noise	0.2
train_interval	The number of steps to run per update	2
learning_rate_v	Learning rate for critic	0.0003
learning_rate_a	Learning rate for actor	0.0001
batch_size	Number of training sequences per update.	16
L	Sequence length for truncated BPTT in training	25

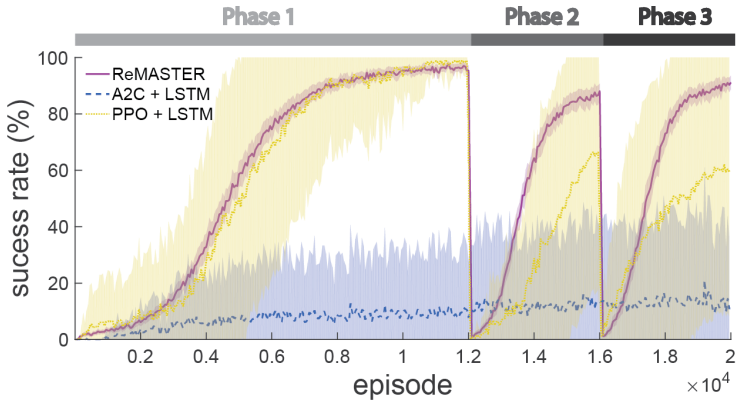

Figure A9: Performance comparison on the consecutive relearning task for ReMASTER and other RL algorithms, plotted in the same way as Fig. 3(b). PPO: proximal policy optimization; A2C: Advantage Actor Critic (on-policy); LSTM: Long short-term memory network. The results of PPO + LSTM and A2C + LSTM were obtained from 10 repeats.

Appendix A5 Comparison with Other RL Algorithms

We also compared the result of ReMASTER to that of a state-of-the-art algorithms (Fig. A9). The yellow dotted curve shows the performance of *PPO + LSTM*, which employed the *proximal policy optimization* (PPO) algorithm [Schulman et al., 2017] with the *long short-term memory* (LSTM) network [Hochreiter and Schmidhuber, 1997] as function approximators for actor and critic. The blue dashed curve indicates the result using A2C[6] with LSTM for approximating value and policy functions. For both A2C + LSTM and PPO + LSTM, we used the *stable-baselines* [Hill et al., 2018] implementation of single-agent RL, using tuned hyper-parameters by grid search (Table A3,A4).

The result shows that A2C + LSTM failed to achieve a comparable performance to ReMASTER, in such a memory-crucial task. However, PPO + LSTM demonstrated results similar to those of the LSTM alternative in Fig. 3 by showing a performance degradation in latter phases. Therefore, we consider that the performance degradation using LSTM is not specific to our algorithm, but is more general case.

[6]The advantage actor-critic (A2C) algorithm [Dhariwal et al., 2017] is a synchronous version of the asynchronous advantage actor-critic (A3C) algorithm [Mnih et al., 2016], while its performance is similar to that of A3C.

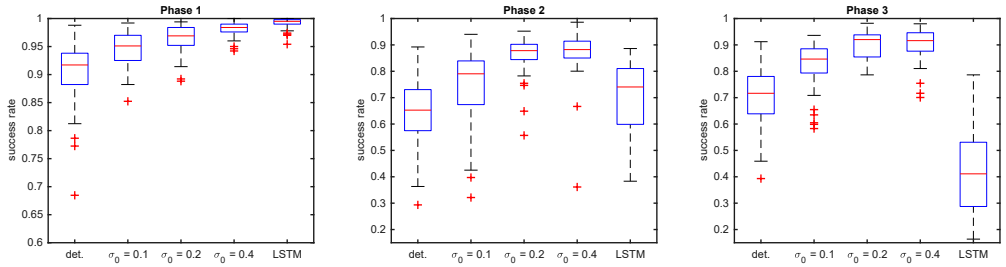

Figure A10: Final performances for different scales of neuronal noise obtained from last 2000 episodes of each phase,. The data were obtain from 50 repeats (same setting as that for Fig.3 in the main paper.

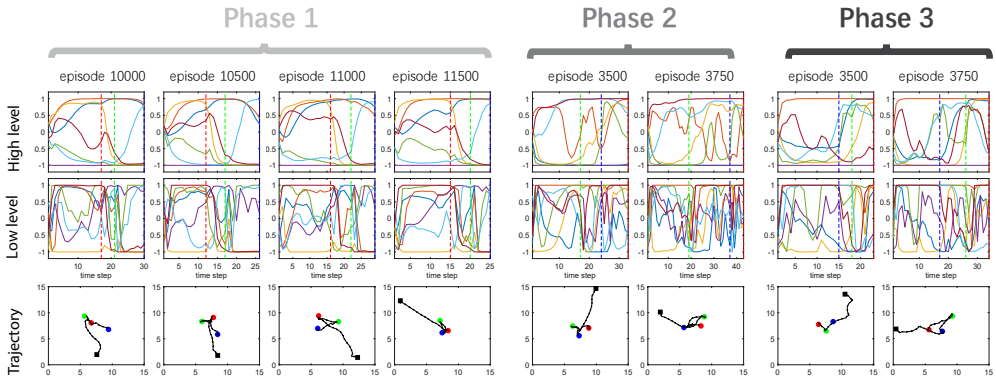

Figure A11: Example episodes showing the behavior of a well-trained ReMASTER agent. Plotted in the same way as Fig.2(c) in the main paper.

Table A3: Hyper-parameters for PPO-LSTM in Fig. A9 using *stable-baselines* [Hill et al., 2018]. A list of values indicates hyper-parameters being searched, where the bold one is selected, which maximizes the mean success rate over all episodes of all phases of the consecutive relearning task.

Hyper-parameter	Description	Value
γ	Discount factor	0.96
ϵ	Clipping range for the PPO objective	0.2
n_steps	The number of steps to run per update	$[32, 64, 128, 256, \mathbf{512}, 1024]$
ent_coef	Entropy coefficient for the loss calculation	$[10^{-5}, 10^{-4}, 10^{-3}, \mathbf{10^{-2}}]$
learning_rate	Learning rate for PPO	$[0.00003, 0.0001, 0.0003, \mathbf{0.001}, 0.003]$
vf_coef	Value function coefficient for the loss calculation	$[0.05, 0.5, \mathbf{5.0}, 50, 500]$
max_grad_norm	The maximum value for the gradient clipping	0.5
noptepochs	Number of epoch when optimizing the surrogate	4
lam	Factor for trade-off of bias vs variance for Generalized Advantage Estimator	0.95
n_MLP	Sizes of hidden layers densely connected for input feature extraction	64, 64
n_LSTM	Layer size of LSTM connecting hidden layers to value and policy outputs	256

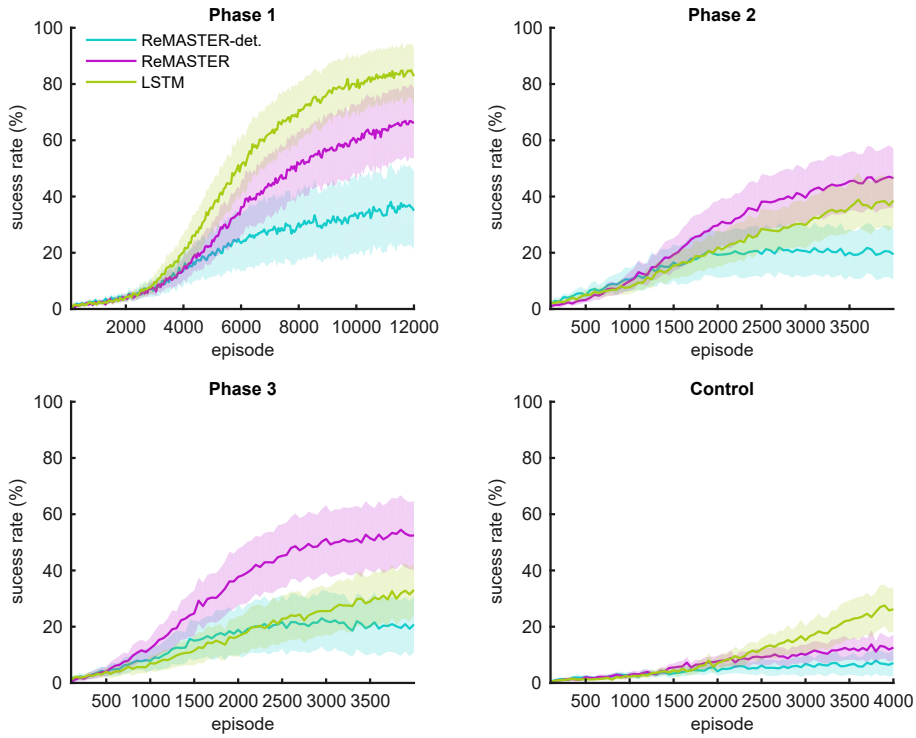

Figure A12: Results on the consecutive relearning task using a range of random hyper-parameters

Table A4: Hyper-parameters for A2C-LSTM in Fig. A9 using *stable-baselines* [Hill et al., 2018]. A list of values indicates hyper-parameters being searched, where the bold one is selected, which maximizes mean success rate over all episodes of all phases of the consecutive relearning task.

Hyper-parameter	Description	Value
γ	Discount factor	0.96
n_steps	The number of steps to run per update	$[\mathbf{16}, 32, 64, 128, 256]$
ent_coef	Entropy coefficient for the loss calculation	$[\mathbf{10^{-4}}, 10^{-3}, 10^{-2}, 10^{-1}]$
learning_rate	Learning rate for A2C	$[0.00003, 0.0001, \mathbf{0.0003}, 0.001, 0.003]$
vf_coef	Value function coefficient for the loss calculation	$[0.05, 0.15, 0.5, \mathbf{1.5}, 5]$
max_grad_norm	The maximum value for the gradient clipping	0.5
n_MLP	Sizes of hidden layers densely connected for input feature extraction	64, 64
n_LSTM	Layer size of LSTM connecting hidden layers to value and policy outputs	256